A Highly Sensitive Biocompatible Spin Probe for Imaging of Oxygen Concentration in Tissues

Anna Bratasz, Aditi C. Kulkarni, and Periannan Kuppusamy
Center for Biomedical EPR Spectroscopy and Imaging, Comprehensive Cancer Center, Davis Heart and Lung Research Institute, Department of Internal Medicine, The Ohio State University, Columbus, Ohio

ABSTRACT The development of an injectable probe formulation, consisting of perchlorotriphenylmethyl triester radical dissolved in hexafluorobenzene, for in vivo oximetry and imaging of oxygen concentration in tissues using electron paramagnetic resonance (EPR) imaging is reported. The probe was evaluated for its oxygen sensitivity, biostability, and distribution in a radiation-induced fibrosarcoma tumor transplanted into C3H mice. Some of the favorable features of the probe are: a single narrow EPR peak (anoxic linewidth, 41 μT), high solubility in hexafluorobenzene (>12 mM), large linewidth sensitivity to molecular oxygen (~1.8 μT/mmHg), good stability in tumor tissue (half-life: 3.3 h), absence of spin-spin broadening (up to 12 mM), and lack of power saturation effects (up to 200 mW). Three-dimensional spatial and spectral-spatial (spectroscopic) EPR imaging measurements were used to visualize the distribution of the probe, as well as to obtain spatially resolved pO_2 information in the mice tumor subjected to normoxic and hyperoxic treatments. The new probe should enable unique opportunities for measurement of the oxygen concentration in tumors using EPR methods.

INTRODUCTION

Physiologists and clinicians define hypoxia as a state of reduced oxygen availability or decreased partial pressure of oxygen (pO_2) below critical thresholds, thus restricting or abolishing the normal function of organs, tissues, or cells (1). In solid tumors, oxygen delivery to the cells is frequently compromised or inhibited due to poor diffusion geometry, severe structural abnormalities of tumor microvessels, and disturbed microcirculation (2). Oxygenation of solid tumors plays a critical role in the development as well as the treatment of tumors. Hypoxia can stimulate angiogenesis (3) or increase the metastatic ability of certain tumors (4,5). Hypoxic cells in tumors are relatively resistant to radiation, chemo-, or photodynamic therapy (6). A number of key findings have emerged on the occurrence of hypoxia in tumors: 1), most tumors have lower median pO_2 than their tissue of origin; 2), many solid tumors contain areas of low pO_2 that cannot be predicted by clinical size, stage, grade, histology, or site; 3), variability in oxygenation between tumors is usually greater than intratumor variability; and 4), recurring tumors have a lower oxygenation status than the corresponding primary tumors. The fact that poorly oxygenated tumors are more aggressive and less susceptible to treatment suggests that tumor oxygenation status is an important parameter for cancer treatment (7,8). Further, the observation of substantial inter- and intratumor heterogeneities among tumors of similar histology and sites further emphasizes the importance of the measurement of hypoxia in individual tumor or patients. In addition, the ability to monitor changes in the pO_2 after treatment could have profound implications in the planning of effective therapeutic strategies (7,8). In particular, radiotherapy could benefit from modulated treatment based on regional variations in pO_2.

The influence of tumor oxygenation on treatment outcome has stimulated the development of a variety of methods for measuring tumor oxygenation (9–11). The methods include: paired-survival curve assays of hypoxic fractions (12), radiation-induced DNA damage measured by ''Comet'' assay (13), cryospectrophotometric measurements of hemoglobin oxygen saturation (14), immuno-histochemical detection of nitroimidazole binding (15), polarographic oxygen electrodes (16), fluorescent and phosphorescent probes based on oxygen-quenching (17,18), and magnetic resonance methods (19–23). The polarographic electrode is the only device approved for clinical use, and although invasive, provides a direct measurement of the oxygen concentration. Magnetic resonance-based methods, such as nuclear magnetic resonance (NMR) and electron paramagnetic resonance (EPR), have the advantage of noninvasive measurement and imaging of oxygen concentration in tissues (19,24,25).

The EPR-based method, known as ''EPR oximetry'', uses oxygen-sensing spin probes whose EPR lines are broadened by molecular oxygen. This approach uses either water-soluble probes such as nitroxyls (26–29) and trityls (21,30–34) that are administered via vascular routes or water-insoluble particulates such as India ink (35,36) and lithium phthalocyanine and derivatives (37–40) that are implanted at desired sites in the tumor. These probes are stable in tissues, nontoxic, and biocompatible. The measurements can be performed noninvasively and repeatedly over periods of months at the same site. There are specific advantages and disadvantages with either approach. The most notable drawbacks are the requirement of systemic administration and poor oxygen sensitivity in the case of soluble probes. For the implanted probes, a notable disadvantage is having to leave

Submitted October 10, 2006, and accepted for publication January 3, 2007.

Address reprint requests to Periannan Kuppusamy, Tel.: 614-292-8998; E-mail: kuppusamy.1@osu.edu.

0006-3495/07/04/2918/08 $2.00

doi: 10.1529/biophysj.106.099135

the particle permanently in the tissue, which may not be desirable for application in humans. Hence, new approaches are sought to circumvent these shortcomings. One approach is to use an implantable and retrievable form of the particulate probes with a suitable coating, encapsulated in oxygen permeable films (41), or to use locally injectable (intratumoral) formulations (42) that may minimize the risk of systemic toxicity. The latter approach has the advantage of using micro-needles for probe delivery to minimize the tissue injury and trauma associated with the placement of the probe. However, to achieve optimal signal intensity, biostability, and oxygen sensitivity of the probe, a diligent choice of the probe formulation is required. This can be achieved using a narrow single line probe dissolved in a nonaqueous solvent having high oxygen solubility and biostability. With this in mind, we have formulated a new probe, a perchlorotriphenylmethyl radical, dissolved in hexafluorobenzene (HFB). We used perchlorotriphenylmethyl-triester radical (PTM-TE, Fig. 1 *A*), which gives a single narrow EPR line (Fig. 1 *B*). The PTM radical and its derivatives are highly stable against a variety of reactive chemical agents, and hence are called ''inert free radicals'' (43,44). They can withstand temperatures as high as 250°C. Their chemical inertness and thermal stability are due to the full steric blockage of the central carbon, where most of the spin density resides (43). HFB has been well established by Mason et al. (19) as a standalone probe for quantitative tumor oximetry using ^{19}F-NMR relaxometry. We report, for the first time, the use of a PTM-TE/HFB formulation for high-resolution oxygen mapping in tumor using EPR spectroscopy. We have investigated the biostability and oxygen sensitivity of the probe in a radiation-induced fibrosarcoma (RIF-1) tumor transplanted in C3H mice. Three-dimensional spatial and spectral-spatial (spectroscopic) EPR imaging measurements have been used to visualize the distribution of the probe, as well as to obtain spatially resolved pO_2 information in the tumor in mice subjected to normoxic and hyperoxic treatments. The results suggest that the new probe formulation enables imaging of the absolute values of oxygen concentration in tumors with remarkable sensitivity under minimally invasive conditions.

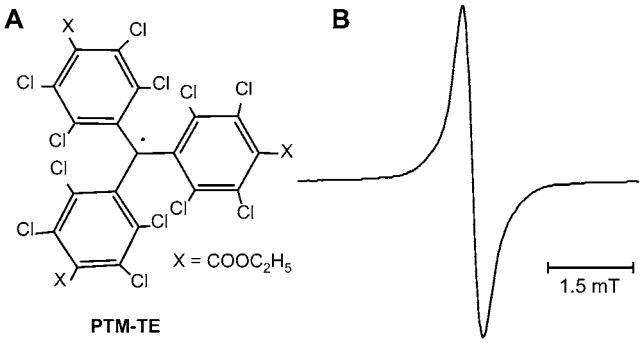

FIGURE 1 (*A*) Chemical structure of perchlorotriphenylmethyl triester radical (PTM-TE) and (*B*) its EPR spectrum in hexafluorobenzene (HFB) measured under room air conditions (20.9% oxygen). The peak-to-peak linewidth is 0.321 mT.

MATERIALS AND METHODS

Reagents

Perchlorotriphenylmethyl radical (PTM-TE) was synthesized as reported (45). Hexafluorobenzene (HFB) was purchased from Apollo Scientific (Stockport, Cheshire, UK).

Calibration of EPR oximetry

PTM-TE was dissolved in HFB to a final concentration of 1 mM and was loaded in a 0.8 mm diameter gas-permeable Teflon tube (Zeus Industrial Products, Orangeburg, SC). The Teflon tube was inserted into a 3-mm quartz EPR tube, which was placed in the resonator. Premixed oxygen and nitrogen gases of known concentrations were flown through the EPR tube attached to a gas flow meter. The oxygen concentration was varied from 0 to 100%. All measurements were taken after equilibrating the sample with the gas mixture. The peak-to-peak linewidth (ΔB_{pp}) of the EPR spectrum were plotted against pO_2 to determine the oxygen sensitivity.

PTM-TE probe properties

The microwave power saturation of the EPR signal, the effect of concentration on the signal intensity and linewidth (spin-spin interaction), and the stability of PTM-TE in HFB were studied at room temperature using X-band (9.8 GHz) EPR spectroscopy.

Animals

Female C3H mice were obtained from the Frederick Cancer Research Center Animal Production Facility (Frederick, MD). The animals were housed five per cage in a climate- and light-controlled room. Food and water were allowed ad libitum. The animals were 50 days old and weighed ~25 g at the time of the experiment. The mice were anesthetized with ketamine and xylazine (i.p.) and inhaled either room air (21% O_2) or carbogen (mixture of 95% O_2 and 5% CO_2) through a nose cone. During the measurements, the body temperature of the animal was monitored using a rectal thermistor probe and maintained at 37 ± 1°C by an infrared lamp placed just above the animal. The experimental protocol used in this study was approved by the Institutional Animal Care and Use Committee of the Ohio State University and conformed to the Guide for the Care and Use of Laboratory Animals (NIH Publication No. 86-23).

RIF-1 tumor growth

Radiation-induced fibrosarcoma-1 (RIF-1) cells were grown in RPMI medium 1640 supplemented with 10% fetal bovine serum and 1% penicillin/streptomycin in an atmosphere of 95% air and 5% CO_2 at 37°C. Cells were trypsinized, centrifuged, and suspended in PBS. The cells (1×10^6) were injected subcutaneously into the upper portion of the right hind limb of C3H mice and grown as solid tumor. All measurements were performed on tumors from 200 to 300 mm^3 in volume.

EPR measurements in tissues

A 15–20 μL aliquot of 12 mM PTM-TE in HFB was injected intramuscularly ($n = 3$) or intratumorally ($n = 3$) at a depth of ~2 mm using 30-gauge

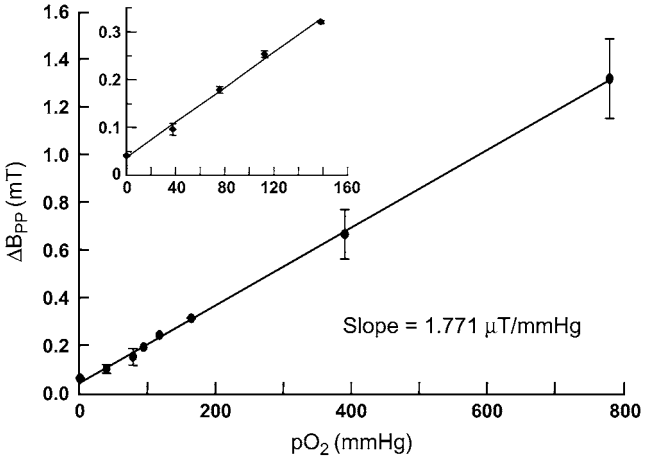

FIGURE 2 Effect of pO_2 on the linewidth of PTM-TE in HFB. The peak-to-peak linewidth of 1 mM PTM-TE in 50 μL of HFB was measured using an X-band EPR spectrometer under different oxygenation conditions as described in Materials and Methods. The linewidth data, expressed as mean $\pm$ SD from three independent measurements, showed a linear variation with pO_2 (*solid line*, $R^2 = 0.98$) with a sensitivity of 1.771 μT/mmHg in the 0–760 mmHg range. The inset shows the dependence of linewidth on oxygen concentration in the physiological range.

needles while the mice were under ketamine/xylazine anesthesia. The oxygen concentration in the normal and tumor tissue was measured using an L-band (1.2 GHz) EPR spectrometer with a loop coil (Magnettech, Berlin, Germany). The frequency of the L-band spectrometer is optimal for animal studies due to microwave absorption and penetration within tissues.

EPR imaging

The in vivo EPR imaging measurements were performed by using a home-built L-band (1.2 GHz) EPR spectrometer with a bridged loop-gap resonator

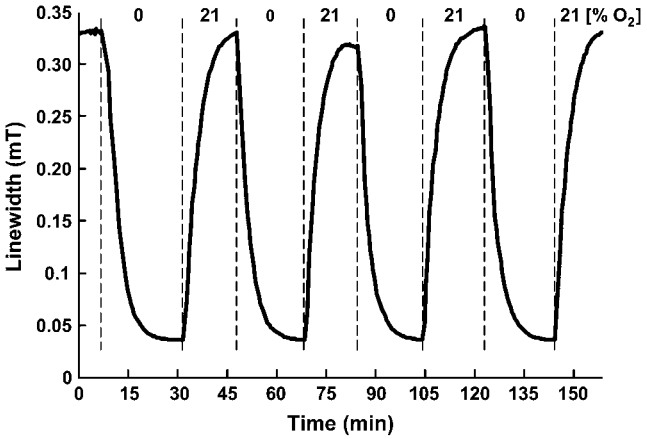

FIGURE 3 Time response of linewidth of PTM-TE in HFB to changes in oxygen concentration. The EPR spectrum of PTM-TE (1 mM PTM-TE in 50 μL HFB) was measured continuously using 5-s scans while the oxygen content in the flowthrough gas mixture was switched between 0% and 21%, at ~15-min cycles, as indicated. The response of the peak-to-peak linewidth, shown as a solid line connecting the measured values to changes in oxygen concentration, was reproducible for several cycles of oxygenation and reoxygenation.

(26). Mapping of the probe (PTM-TE) location and the oxygen concentration in the tumor was obtained by spatial and spectroscopic (spectral-spatial) EPR imaging methods that are well established in our laboratory (26,37). The principle of EPR mapping of pO_2 is based on the oxygen-dependent linewidth data from each voxel in the object. A notable caveat is that the pO_2 information can only be obtained from those voxels that have measurable EPR signal intensity. Thus pO_2 values are not obtained from those voxels within the field of view (FOV) that either have no signal, or signal intensities less than threshold set at 30% of maximum signal intensity. The voxels with undetermined pO_2 values are coded with black color. The following parameters were used for EPR image acquisition: sweep time, 4 s; modulation amplitude, 18 μT; time constant, 0.04 s; microwave power, 5 mW; FOV, 20 mm; number of projections, 144 or 256. The sweep width was 1 mT for spatial imaging while it was variable for spectroscopic (spectral-spatial) imaging. The spectroscopic imaging used a spectral window ((FOV) of 0.5 mT. Computer software based on MatLab Software (The MathWorks,

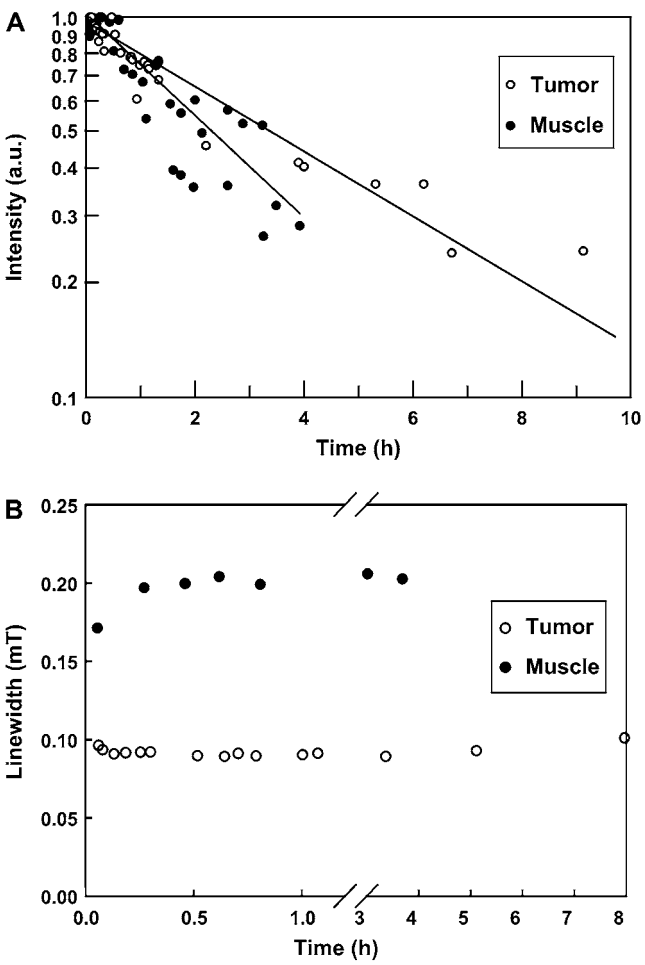

FIGURE 4 Stability of PTM-TE in normal and tumor tissues. A small volume (20 μL) of 12 mM PTM-TE in HFB was injected directly into muscle or RIF-1 tumors grown in the hind leg of C3H mice and the intensity of the EPR signal was continuously measured using an L-band EPR spectrometer for up to 10 h. The plot (*A*) shows the time-course of EPR intensity data (relative to respective initial reading, displayed on a logarithmic scale) obtained from three mice per group. The decay half-life of PTM-TE was 3.3 $\pm$ 0.4 h in tumor and 2.3 $\pm$ 0.5 h in muscle. The plot (*B*) shows changes in the linewidth of the EPR signal during the measurement period. No significant change in the linewidth was observed.

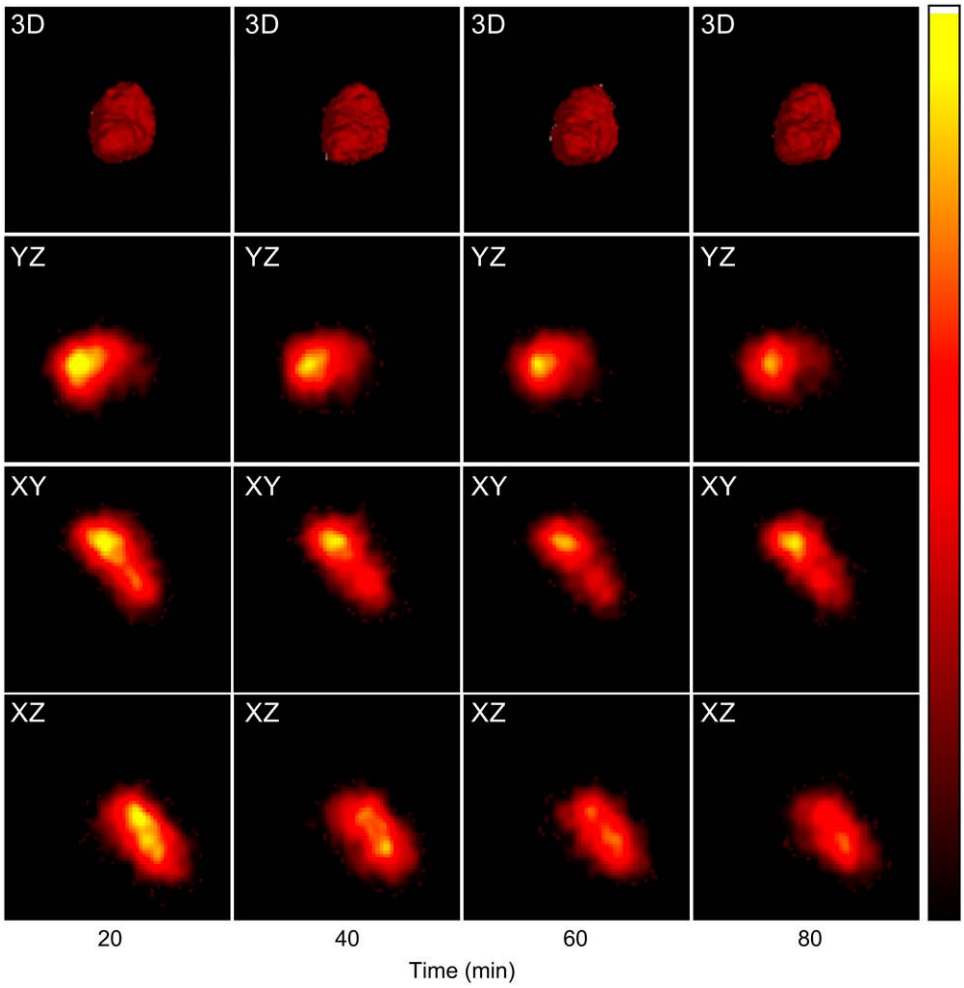

FIGURE 5 Three-dimensional images of the distribution of PTM-TE in tumor as a function of time. A solution of 12 mM PTM-TE in HFB (20 μL) was directly injected into a RIF-1 tumor grown in the hind limb of C3H mice at a depth of ~2 mm using a 30-gauge needle. Three-dimensional spatial EPR images were obtained as a function of time as indicated. The top panels ($20 \times 20 \times 20$ mm^3) show the time-course visualization of three-dimensional images at 30% background transparency. The following three rows show the time-course images of PTM-TE in three orthogonal slices (*XY*, *YZ*, and *ZX*) intersecting at the center of the three-dimensional image. The images were reconstructed from 256 projections, acquired using a magnetic field gradient of 250 mT/m.

Natick, MA) was developed to compute pO_2 values from the image data. The calibration curve was corrected according to linewidth values obtained at room air and under anoxic conditions using the L-band EPR spectrometer. The software used an automated fitting of the lineshape data to a Lorentzian function and converted the linewidth to pO_2 using a standard oximetry curve. The output of the result was a 256 color-coded 64×64 grid image of pO_2. A linear interpolation was used in the hardcopy (high-resolution) representation of the images.

Statistical analysis

Data are expressed as mean ± standard deviation (SD). Comparisons among groups were performed using the Student's *t*-test with the level of significance (*P*) set at 0.05.

RESULTS AND DISCUSSION

EPR properties of PTM-TE

PTM-TE is insoluble in aqueous solutions. However, it is soluble in many nonpolar solvents including HFB. PTM-TE in HFB exhibits a single line EPR peak with a peak-to-peak linewidth (ΔB_{pp}) of 0.321 mT under indoor ambient conditions (Fig. 1 *B*). The linewidth is highly sensitive to the concentration of molecular oxygen in the solution. As shown in Fig. 2, the linewidth of PTM-TE exhibits a linear relationship with pO_2 in the measured range of 0–760 mmHg. The sensitivity of oxygen-induced line-broadening is 1.771 μT/mmHg, which is >50 times higher than that of water-soluble nitroxyls and trityls (34). This value is also higher when compared to the sensitivity of particulate probes such as lithium phthalocyanine (38,39) and lithium butoxynaphthalocyanine (40). The high sensitivity of the formulation for oxygen can be due to the high solubility of oxygen in HFB. The solubility at atmospheric pressure (21% of oxygen) at 25°C is 270 μM in water and 4400 μM in HFB (46). No spin-spin broadening was observed for up to a 12 mM concentration (solubility limit) of PTM in HFB (data not shown). Power saturation studies demonstrated that the anoxic spectrum was not significantly saturated up to 1 mW of incident power (at 9.78 GHz), while the spectrum in normoxic (room air-equilibrated, $\Delta B_{pp} = 321$ μT) solutions was not saturated up to 200 mW (data not shown). The radical was observed to be stable in HFB in the dark. However, in the presence of visible or UV light, a decay of

the EPR signal was observed. However, light had no effect on the oxygen-sensing characteristics of the probe.

The time-response of the linewidth to acute changes in oxygen concentration was evaluated by continuously measuring the EPR spectrum of PTM-TE (1 mM in 50 μL of HFB contained in a gas-permeable Teflon tubing), while the oxygen content in the flowthrough gas mixture was switched between 0% and 21%. The response of the peak-to-peak linewidth to changes in oxygen concentration was highly reproducible for several cycles of deoxygenation and reoxygenation (Fig. 3). No significant differences in the rates of change in linewidth were observed between the oxygenation ($t_{1/2} = 2.3 \pm 0.5$ min) and deoxygenation ($t_{1/2} = 2.5 \pm 0.3$ min) processes.

Stability and distribution of PTM-TE in tissue

To evaluate the stability of the probe solution in normal tissue and tumor, a 20 μL solution of 12 mM PTM-TE in HFB was directly injected into muscle or RIF-1 tumors using a 30-gauge needle at a depth of ~2 mm. The animals were placed in the L-band EPR resonator and the decay of the PTM-TE signal intensity was measured for up to 9 h post-injection. As shown in Fig. 4 *A*, the intensity of the EPR signal decreased with time. The data were suggestive of an exponential decay with a half-life of 3.3 ± 0.4 h in the tumor tissue and 2.3 ± 0.5 h in muscle. To address the possibility of diffusion of PTM-TE out of the HFB vehicle into endogenous environments with different oxygen solubility we monitored the linewidth data of PTM-TE/HFB in the normal muscle and tumor tissue. As shown in Fig. 4 *B*, there was no significant change in linewidth during the 8-h observation period, suggesting that the probe did not diffuse out of HFB.

The three-dimensional distribution of PTM-TE/HFB fluid in the solid tumor was determined by EPR imaging. A solution of 12 mM PTM-TE in HFB (20 μL) was directly injected into the 200–300 mm^3 transplanted RIF-1 tumors. The animals were placed in the L-band EPR resonator and three-dimensional spatial EPR images were obtained. Fig. 5 shows the time-course images of PTM-TE distribution in a tumor (of ~200 mm^3 volume) obtained at 20-min intervals for 80 min. The maximum volume of distribution of the image at the 30% background threshold cutoff was estimated to be 29.3 mm^3, which is ~15% of the tumor size. It was observed from the three-dimensional image, as well as from the change in the concentration of PTM-TE in the three orthogonal slices shown as a function of time, that the volume of distribution was fairly unchanged with time. This suggests that the signal decay may be primarily due to loss of PTM-TE and not due to diffusion or clearance of the carrier (HFB) from the site of observation. This observation was also consistent with the longer decay half-life of HFB in tumor tissue (20). Mason et al. (19) have reported that after intratumoral injection in a Dunning prostate tumor in a rat, HFB is distributed in the form of fine droplets, while our images showed the presence of a continuous distribution. The appearance of a continuous distribution in our study may be attributed to the poor spatial resolution (~0.5 mm) of the image, which was mainly due to poor signal/noise ratio of the signal. Assuming that 20 μL of 12 mM PTM-TE was distributed in a volume of 29.3 mm^3, the effective concentration of the paramagnetic probe was estimated to be only 8 μM in the tissue. This explains the absence of discrete regions of PTM-TE in the EPR images. This limitation can be overcome using larger volume of the probe or by using fewer acquisitions to obtain a higher signal/noise ratio.

Tumor pO_2 and its dependence on FiO_2

To check the effect of modulation of fractional percentage of inspired oxygen (FiO_2) on the tumor pO_2 measured using the peak-to-peak linewidth of the EPR spectrum, experiments were performed in tumor-bearing mice under normal (air-breathing) and hyperoxygenated (carbogen-breathing) conditions. A solution of 12 mM PTM-TE in 20 μL of HFB was directly injected into the tumor and the tumor oxygenation was continuously measured during cycles of air- and carbogen-breathing. A representative time-course measurement of tumor

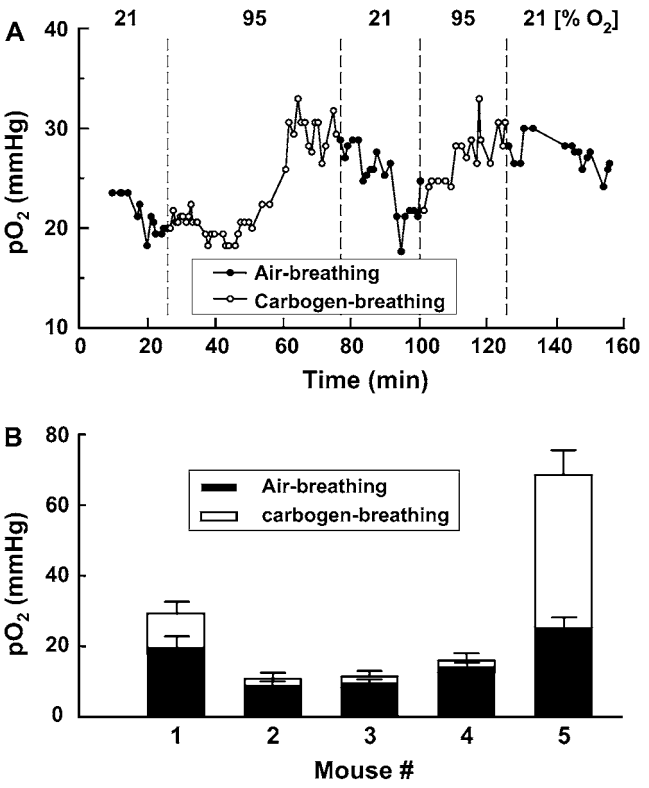

FIGURE 6 Effect of FiO_2 on the tumor pO_2. A solution of 20 microliters of PTM-TE (12 mM in HFB) was injected directly into RIF-1 tumor grown in the hind leg of a C3H mouse. (*A*) Change in pO_2 in the tumor of a single animal while the FiO_2 was successively switched between 21% and 95% (carbogen gas), as indicated. (*B*) The pO_2 values obtained before (FiO_2 = 21%) and 20 min after changing the FiO_2 to 95% in five different animals.

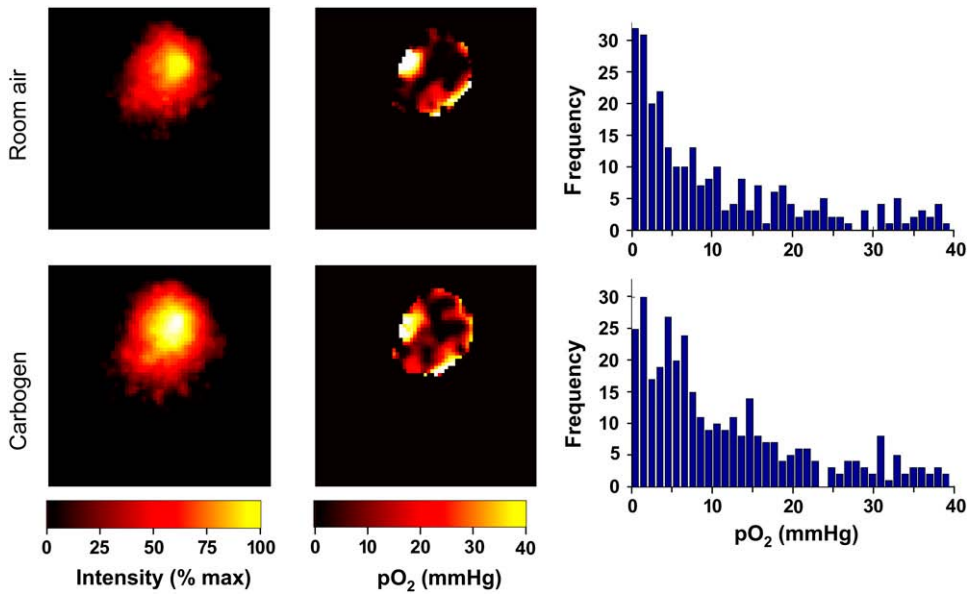

FIGURE 7 Images of the distribution of PTM-TE and oxygen concentration in tumor. A 20-μL solution of 12 mM PTM-TE in HFB was directly injected into a RIF-1 tumor (size = 200 mm^3), grown in the hind limb of C3H mice, at a depth of ~2 mm using a 30-gauge needle and three-dimensional spectral-spatial (spectroscopic) EPR images were obtained while the animal was breathing either room air or carbogen gas. The images (15 × 15 mm^2) were reconstructed from 144 projections acquired using a maximum magnetic field gradient of 500 mT/m. The probe is distributed in ~10% of the tumor. Note that the oxygen information is obtained only from the regions where the probes are present. The pO_2 values in the air-breathing animal are hypoxic (mean pO_2 = 10.6 mmHg; median pO_2 = 5.0 mmHg) and significantly right-skewed. Carbogen-breathing increased both the mean and median pO_2 values (mean pO_2 = 11.7 mmHg; median pO_2 = 6.9 mmHg) in the tumor.

pO_2 is shown in Fig. 6 *A*. The tumor pO_2 increased during carbogen-breathing and the effect of cycling between normal and hyperoxygenated gas was fairly reproducible, although the exact rates and levels of oxygenation were not the same between the cycles. It is well known that tumor oxygenation and its change during hyperoxic challenge are highly variable depending on the site of examination in the tumor (19,47). This was also evident from the results of the above measurements in five different animals shown in Fig. 6 *B*, where both the normoxic and hyperoxic treatments demonstrated different levels of oxygenation.

Since the RIF-1 tumors are known to have significant heterogeneity in oxygenation (48), the 15% volume covered by the probe is expected to have nonuniform regions of oxygenation. Hence, a spectroscopic determination (single readout) of pO_2 may reveal only a single value, which is often an overestimate of the hypoxic value due to the use of peak-to-peak linewidth. Hence, one needs to use imaging methods to resolve, spatially, the regional differences in the oxygenation.

Mapping of pO_2 distribution in the tumor

To resolve the oxygen distribution within the region of PTM-TE/HFB in the tumor, we performed three-dimensional spectroscopic imaging. The tumor-bearing mice were allowed to breathe room air and the EPR spectral-spatial images were collected. Then the same animals were allowed to breathe carbogen gas (95% O_2 and 5% CO_2) for 20 min before images were collected. The spatial and oxygen images obtained under these two conditions are shown in Fig. 7. The pO_2 data from the tumor of an air-breathing mouse showed significant distribution both in the magnitude and frequency of occurrence within the examined volume. In general, the values were hypoxic (mean pO_2 = 10.6 mmHg; median pO_2 = 5.0 mmHg) and right-skewed, which is characteristic of this type of tumor (49). Carbogen-breathing by the mouse increased both the mean and median tumor pO_2 values (mean pO_2 = 11.7 mmHg; median pO_2 = 6.9 mmHg).

HFB is well characterized in terms of a lack of toxicity, exhibiting no mutagenicity, teratogenicity, or fetotoxicity (50). The Material Safety Data Sheet indicates $LD_{50} > 25$ g/kg (oral administration in rat) and LC_{50} 95 g/m^3/2h (inhalation by mouse). HFB had been proposed as a veterinary anesthetic and has been used in many species including ponies, sheep, cats, dogs, rats, and mice, but was abandoned due to its high volatility (boiling point 81°C) and low flash point (10°C) (51,52). Song et al. (53) have established HFB as a stand-alone probe for quantitative tumor oximetry using ^{19}F-NMR relaxometry and echo planar magnetic resonance imaging (MRI). The MRI measurements using HFB in Dunning prostate tumors in rats revealed significant right-skewness with low mean pO_2, when animals were breathing 33% oxygen, which increased with a rise in the FiO_2 in the breathing gas (54). Since this formulation consisted of a combination of EPR oximetry probe, PTM-TE, and NMR/MRI oximetry probe, HFB, it is also possible to perform multimodality (EPRI/MRI) oxygen imaging as well as anatomical map (MRI) with minimal invasiveness and systemic toxicity.

We thank Dr. Christophe Buron for synthesis of the PTM-TE probe and Brian Rivera for critical reading of the manuscript.

We acknowledge financial support from National Institutes of Health grants No. CA 78886 and No. EB004031.

REFERENCES

1. Zander, R., and P. Vaupel. 1985. Proposal for using a standardized terminology on oxygen transport to tissue. *Adv. Exp. Med. Biol.* 191:965–970.
2. Vaupel, P., F. Kallinowski, and P. Okunieff. 1989. Blood flow, oxygen and nutrient supply, and metabolic microenvironment of human tumors: a review. *Cancer Res.* 49:6449–6465.
3. Shweiki, D., A. Itin, D. Soffer, and E. Keshet. 1992. Vascular endothelial growth factor induced by hypoxia may mediate hypoxia-initiated angiogenesis. *Nature.* 359:843–845.
4. Brizel, D. M., S. P. Scully, J. M. Harrelson, L. J. Layfield, J. M. Bean, L. R. Prosnitz, and M. W. Dewhirst. 1996. Tumor oxygenation predicts for the likelihood of distant metastases in human soft tissue sarcoma. *Cancer Res.* 56:941–943.
5. Rofstad, E. K. 2000. Microenvironment-induced cancer metastasis. *Int. J. Radiat. Biol.* 76:589–605.
6. Gray, L. H., A. D. Conger, M. Ebert, S. Hornsey, and O. C. Scott. 1953. The concentration of oxygen dissolved in tissues at the time of irradiation as a factor in radiotherapy. *Br. J. Radiol.* 26:638–648.
7. Menon, C., and D. L. Fraker. 2005. Tumor oxygenation status as a prognostic marker. *Cancer Lett.* 221:225–235.
8. Evans, S. M., and C. J. Koch. 2003. Prognostic significance of tumor oxygenation in humans. *Cancer Lett.* 195:1–16.
9. Stone, H. B., J. M. Brown, T. L. Phillips, and R. M. Sutherland. 1993. Oxygen in human tumors: correlations between methods of measurement and response to therapy. Summary of a workshop held November 19–20, 1992, at the National Cancer Institute, Bethesda, Maryland. *Radiat. Res.* 136:422–434.
10. Milosevic, M., A. Fyles, D. Hedley, and R. Hill. 2004. The human tumor microenvironment: invasive (needle) measurement of oxygen and interstitial fluid pressure. *Semin. Radiat. Oncol.* 14:249–258.
11. Olive, P. L., and C. Aquino-Parsons. 2004. Measurement of tumor hypoxia using single-cell methods. *Semin. Radiat. Oncol.* 14: 241–248.
12. Dorie, M. J., and R. F. Kallman. 1984. Reoxygenation in the RIF-1 tumor. *Int. J. Radiat. Oncol. Biol. Phys.* 10:687–693.
13. Olive, P. L. 1994. Radiation-induced reoxygenation in the SCCVII murine tumor: evidence for a decrease in oxygen consumption and an increase in tumor perfusion. *Radiother. Oncol.* 32:37–46.
14. Mueller-Klieser, W., P. Vaupel, R. Manz, and R. Schmidseder. 1981. Intracapillary oxyhemoglobin saturation of malignant tumors in humans. *Int. J. Radiat. Oncol. Biol. Phys.* 7:1397–1404.
15. Koch, C. J. 2002. Measurement of absolute oxygen levels in cells and tissues using oxygen sensors and 2-nitroimidazole EF5. *Methods Enzymol.* 352:3–31.
16. Hockel, M., K. Schlenger, C. Knoop, and P. Vaupel. 1991. Oxygenation of carcinomas of the uterine cervix: evaluation by computerized O_2 tension measurements. *Cancer Res.* 51:6098–6102.
17. Vinogradov, S. A., L. W. Lo, W. T. Jenkins, S. M. Evans, C. Koch, and D. F. Wilson. 1996. Noninvasive imaging of the distribution in oxygen in tissue in vivo using near-infrared phosphors. *Biophys. J.* 70:1609–1617.
18. Braun, R. D., J. L. Lanzen, S. A. Snyder, and M. W. Dewhirst. 2001. Comparison of tumor and normal tissue oxygen tension measurements using OxyLite or microelectrodes in rodents. *Am. J. Physiol. Heart Circ. Physiol.* 280:H2533–H2544.
19. Mason, R. P., S. Hunjan, D. Le, A. Constantinescu, B. R. Barker, P. S. Wong, P. Peschke, E. W. Hahn, and P. P. Antich. 1998. Regional tumor oxygen tension: fluorine echo planar imaging of hexafluorobenzene reveals heterogeneity of dynamics. *Int. J. Radiat. Oncol. Biol. Phys.* 42:747–750.
20. Zhao, D., L. Jiang, and R. P. Mason. 2004. Measuring changes in tumor oxygenation. *Methods Enzymol.* 386:378–418.
21. Elas, M., B. B. Williams, A. Parasca, C. Mailer, C. A. Pelizzari, M. A. Lewis, J. N. River, G. S. Karczmar, E. D. Barth, and H. J. Halpern. 2003. Quantitative tumor oxymetric images from 4D electron paramagnetic resonance imaging (EPRI): methodology and comparison with blood oxygen level-dependent (BOLD) MRI. *Magn. Reson. Med.* 49:682–691.
22. Swartz, H. M. 2004. Using EPR to measure a critical but often unmeasured component of oxidative damage: oxygen. *Antioxid. Redox. Signal.* 6:677–686.
23. Gallez, B., C. Baudelet, and B. F. Jordan. 2004. Assessment of tumor oxygenation by electron paramagnetic resonance: principles and applications. *NMR Biomed.* 17:240–262.
24. Dunn, J. F., J. A. O'Hara, Y. Zaim-Wadghiri, H. Lei, M. E. Meyerand, O. Y. Grinberg, H. Hou, P. J. Hoopes, E. Demidenko, and H. M. Swartz. 2002. Changes in oxygenation of intracranial tumors with carbogen: a BOLD MRI and EPR oximetry study. *J. Magn. Reson. Imaging.* 16:511–521.
25. Krishna, M. C., S. English, K. Yamada, J. Yoo, R. Murugesan, N. Devasahayam, J. A. Cook, K. Golman, J. H. Ardenkjaer-Larsen, S. Subramanian, and J. B. Mitchell. 2002. Overhauser enhanced magnetic resonance imaging for tumor oximetry: co-registration of tumor anatomy and tissue oxygen concentration. *Proc. Natl. Acad. Sci. USA.* 99:2216–2221.
26. Kuppusamy, P., M. Afeworki, R. A. Shankar, D. Coffin, M. C. Krishna, S. M. Hahn, J. B. Mitchell, and J. L. Zweier. 1998. In vivo electron paramagnetic resonance imaging of tumor heterogeneity and oxygenation in a murine model. *Cancer Res.* 58:1562–1568.
27. Baker, J. E., W. Froncisz, J. Joseph, and B. Kalyanaraman. 1997. Spin label oximetry to assess extracellular oxygen during myocardial ischemia. *Free Radic. Biol. Med.* 22:109–115.
28. Glockner, J. F., H. C. Chan, and H. M. Swartz. 1991. In vivo oximetry using a nitroxide-liposome system. *Magn. Reson. Med.* 20:123–133.
29. Froncisz, W., C. S. Lai, and J. S. Hyde. 1985. Spin-label oximetry: kinetic study of cell respiration using a rapid-passage T1-sensitive electron spin resonance display. *Proc. Natl. Acad. Sci. USA.* 82:411–415.
30. Ardenkjaer-Larsen, J. H., I. Laursen, I. Leunbach, G. Ehnholm, L. G. Wistrand, J. S. Petersson, and K. Golman. 1998. EPR and DNP properties of certain novel single electron contrast agents intended for oxymetric imaging. *J. Magn. Reson.* 133:1–12.
31. Matsumoto, K., S. English, J. Yoo, K. Yamada, N. Devasahayam, J. A. Cook, J. B. Mitchell, S. Subramanian, and M. C. Krishna. 2004. Pharmacokinetics of a triarylmethyl-type paramagnetic spin probe used in EPR oximetry. *Magn. Reson. Med.* 52:885–892.
32. Matsumoto, K., S. Subramanian, N. Devasahayam, T. Aravalluvan, R. Murugesan, J. A. Cook, J. B. Mitchell, and M. C. Krishna. 2006. Electron paramagnetic resonance imaging of tumor hypoxia: Enhanced spatial and temporal resolution for in vivo pO_2 determination. *Magn. Reson. Med.* 55:1157–1163.
33. Rizzi, C., A. Samouilov, V. K. Kutala, N. L. Parinandi, J. L. Zweier, and P. Kuppusamy. 2003. Application of a trityl-based radical probe for measuring superoxide. *Free Radic. Biol. Med.* 35:1608–1618.
34. Williams, B. B., H. al Hallaq, G. V. Chandramouli, E. D. Barth, J. N. Rivers, M. Lewis, V. E. Galtsev, G. S. Karczmar, and H. J. Halpern. 2002. Imaging spin probe distribution in the tumor of a living mouse with 250 MHz EPR: correlation with BOLD MRI. *Magn. Reson. Med.* 47:634–638.
35. Khan, N., H. Hou, P. Hein, R. J. Comi, J. C. Buckey, O. Grinberg, I. Salikhov, S. Y. Lu, H. Wallach, and H. M. Swartz. 2005. Black magic and EPR oximetry: From lab to initial clinical trials. *Adv. Exp. Med. Biol.* 566:119–125.
36. Nakashima, T., F. Goda, J. Jiang, T. Shima, and H. M. Swartz. 1995. Use of EPR oximetry with India ink to measure the pO_2 in the liver in vivo in mice. *Magn. Reson. Med.* 34:888–892.
37. Ilangovan, G., A. Bratasz, H. Li, P. Schmalbrock, J. L. Zweier, and P. Kuppusamy. 2004. In vivo measurement and imaging of tumor

oxygenation using co-embedded paramagnetic particulates. *Magn. Reson. Med.* 52:650–657.

38. Ilangovan, G., H. Li, J. L. Zweier, M. C. Krishna, J. B. Mitchell, and P. Kuppusamy. 2002. In vivo measurement of regional oxygenation and imaging of redox status in RIF-1 murine tumor: effect of carbogen-breathing. *Magn. Reson. Med.* 48:723–730.
39. Liu, K. J., P. Gast, M. Moussavi, S. W. Norby, N. Vahidi, T. Walczak, M. Wu, and H. M. Swartz. 1993. Lithium phthalocyanine: a probe for electron paramagnetic resonance oximetry in viable biological systems. *Proc. Natl. Acad. Sci. USA.* 90:5438–5442.
40. Pandian, R. P., N. L. Parinandi, G. Ilangovan, J. L. Zweier, and P. Kuppusamy. 2003. Novel particulate spin probe for targeted determination of oxygen in cells and tissues. *Free Radic. Biol. Med.* 35: 1138–1148.
41. Dinguizli, M., S. Jeumont, N. Beghein, J. He, T. Walczak, P. N. Lesniewski, H. Hou, O. Y. Grinberg, A. Sucheta, H. M. Swartz, and B. Gallez. 2006. Development and evaluation of biocompatible films of polytetrafluoroethylene polymers holding lithium phthalocyanine crystals for their use in EPR oximetry. *Biosens. Bioelectron.* 21:1015–1022.
42. Liu, K. J., M. W. Grinstaff, J. Jiang, K. S. Suslick, H. M. Swartz, and W. Wang. 1994. In vivo measurement of oxygen concentration using sonochemically synthesized microspheres. *Biophys. J.* 67:896–901.
43. Ballester, M., C. Miravitlles, E. Molins, and C. Carreras. 2003. Oxidation of the perchlorotriphenylmethyl radical to the carbocation, and its unique abrupt reversion. *J. Org. Chem.* 68:2748–2751.
44. Ballester, M., J. Riera, J. Castafier, C. Badia, and J. M. Monso. 1971. Inert carbon free radicals. I. Perchlorodiphenylmethyl and perchlorotriphenylmethyl radical series. *J. Am. Chem. Soc.* 93:2215–2225.
45. Ballester, M. 1986. An easy, high-yield synthesis of highly chlorinated monoarylmethanes, diarylmethanes and triarylmethanes. *Synthesis* (*Mass.*). 1:64–66.
46. Murov, S. L., G. L. Hug, and I. Carmichael. 1993. Handbook of Photochemistry. M. Dekker, New York.
47. Mason, R. P., W. Rodbumrung, and P. P. Antich. 1996. Hexafluorobenzene: a sensitive 19F NMR indicator of tumor oxygenation. *NMR Biomed.* 9:125–134.
48. Pogue, B. W., K. D. Paulsen, J. A. O'Hara, C. M. Wilmot, and H. M. Swartz. 2001. Estimation of oxygen distribution in RIF-1 tumors by diffusion model-based interpretation of pimonidazole hypoxia and Eppendorf measurements. *Radiat. Res.* 155:15–25.
49. Adam, M. F., M. J. Dorie, and J. M. Brown. 1999. Oxygen tension measurements of tumors growing in mice. *Int. J. Radiat. Oncol. Biol. Phys.* 45:171–180.
50. Rietjens, I. M., A. Steensma, C. Den Besten, G. van Tintelen, J. Haas, B. van Ommen, and P. J. van Bladeren. 1995. Comparative biotransformation of hexachlorobenzene and hexafluorobenzene in relation to the induction of porphyria. *Eur. J. Pharmacol.* 293:293–299.
51. Hall, L. W., and S. R. Jackson. 1973. Hexafluorobenzene. Further studies as an anaesthetic agent. *Anaesthesia.* 28:155–159.
52. Burns, T. H., J. M. Hall, A. Bracken, and G. Gouldstone. 1961. An investigation of new fluorine compounds in anaesthesia. III. The anaesthetic properties of hexafluorobenzene. *Anaesthesia.* 16: 333–339.
53. Song, Y., K. L. Worden, X. Jiang, D. Zhao, A. Constantinescu, H. Liu, and R. P. Mason. 2003. Tumor oxygen dynamics: comparison of 19F MR EPI and frequency domain NIR spectroscopy. *Adv. Exp. Med. Biol.* 530:225–236.
54. Zhao, D., A. Constantinescu, E. W. Hahn, and R. P. Mason. 2002. Differential oxygen dynamics in two diverse Dunning prostate R3327 rat tumor sublines (MAT-Lu and HI) with respect to growth and respiratory challenge. *Int. J. Radiat. Oncol. Biol. Phys.* 53: 744–756.